Journal of Power Sources 268 (2014) 404–413

Contents lists available at ScienceDirect

Journal of Power Sources

journal homepage: www.elsevier.com/locate/jpowsour

Effect of CO_2 on the stability of strontium doped lanthanum manganite cathode

Boxun Hu [a], Manoj K. Mahapatra [a, *], Michael Keane [a], Heng Zhang [b], Prabhakar Singh [a, b]

[a] Center for Clean Energy Engineering, Department of Materials Science and Engineering, University of Connecticut, USA
[b] Institute of Materials Science, University of Connecticut, USA

HIGHLIGHTS

- Formation of strontium carbonate on the LSM surface decreases the electrochemical performance.
- LSM cathode performance during exposure to CO_2–air shows initial degradation.
- LSM cathode activated in air shows subsequent negligible degradation in CO_2–air.
- Effect of CO_2 on the LSM stability is less pronounced than that of H_2O.

ARTICLE INFO

Article history:
Received 3 April 2014
Received in revised form
9 June 2014
Accepted 9 June 2014
Available online 17 June 2014

Keywords:
Lanthanum strontium manganite
Carbon dioxide
Strontium carbonate
Solid oxide fuel cell
Cathodic activation

ABSTRACT

Strontium doped lanthanum manganite cathode stability in 0–10% carbon dioxide containing air has been studied in the temperature range of 1023–1123 K with cathodic biases of 0 V and 0.5 V. The current density of the LSM cathode remains stable after an initial decrease. Surface analyses of the pre-test and post-test LSM cathodes using Auger electron spectroscopy (AES) and attenuated total reflectance-Fourier transform infrared spectroscopy (ATR-FTIR) techniques suggest that the formation of $SrCO_3$ at the LSM surface leads to initial performance degradation. Our observations also indicate that CO_2 does not affect the current density after an initial LSM activation in air. Overall, the LSM performance degradation in CO_2-containing air is less severe than in humidified air.

1. Introduction

Fuel flexibility, high efficiency, and negligible emission of pollutants make solid oxide fuel cell (SOFC) technology viable to address energy security and environmental sustainability [1]. Despite tremendous progress in the past decades [2,3], SOFC systems are yet to fully penetrate commercial markets due to high cost and performance degradation over the entire operational period (~5000 h for auxiliary power applications and ≥40,000 h for large scale stationary applications). The relative stability of the component materials of SOFC systems during device fabrication and operation determines their reliability and performance degradation. The bulk, interface, and surface stability of the SOFC cathodes are significant contributors to the performance degradation [4,5].

Strontium (20 mol%) doped lanthanum manganite (LSM) has been considered as the state-of-the-art cathode for an SOFC operating above 1073 K due to the desirable thermo-physical properties [6]. However, the LSM cathode suffers degradation under operational conditions due to aging as well as interaction with the zirconia electrolyte and impurities in the cathode gas atmosphere [7,8]. Formation of electrochemically insulating $La_2Zr_2O_7$ with exolution of Mn from LSM lattice is commonly observed at the interface of LSM and zirconia electrolyte [9–12]. $La_2Zr_2O_7$ at the interface decreases the electrochemically active (triple phase boundary) area. The nominal intrinsic impurities in cathode gas include ~3% H_2O, ~400 ppm CO_2 [13] and 0.05–0.15 ppm SO_2 [14] in air. Chromium vapor species from the metallic interconnects and balance of plant (BOP) components and silicon vapor species from sealing materials are the general extrinsic impurities in cathode gas

* Corresponding author. 44 Weaver Road, Storrs Mansfield, CT 06269-5233, USA. Tel.: +1 860 486 4284; fax: +1 860 486 8378.
E-mail addresses: mkmanoj@engr.uconn.edu, mkmanoj78@gmail.com (M.K. Mahapatra).

http://dx.doi.org/10.1016/j.jpowsour.2014.06.044
0378-7753/

stream [12,15]. The chromium vapor species randomly deposit as Cr_2O_3 and also react with LSM to form chromium manganese spinel preferably at electrochemically active sites due to energetics [6,12]. Similarly, vapor species from sealing material can also deposit as oxides and reacts chromium oxide to form alkali chromates [6,15]. Besides decrease in the electrochemically active sites, formation of these secondary phases also changes the morphologies and compositional heterogeneity in the cathode and the interface. Moreover, manganese diffusion into the zirconia electrolyte and the thermal expansion mismatch of the $La_2Zr_2O_7$ with the LSM and zirconia lead to poor contact between electrolyte and cathode [8,10].

Cathode performance also depends on the oxygen reduction and transport kinetics at the cathode surface [16,17]. The oxygen reduction reaction (ORR) at the LSM involves adsorption of oxygen molecules at surface followed by desorption, surface diffusion of oxygen, and ionization of oxygen (charge transfer) [18]. Insulating oxides at the cathode surface block active ORR sites and decrease the oxygen reduction and transport kinetics. Strontium oxide phase, the inactive sites in LSM for oxygen reduction, is often observed in as-fabricated perovskite cathode surface due to surface energetics [19,20]. The intrinsic impurities in the real world cathode gas stream influences the ORR by favoring SrO segregation and competing with the oxygen for the active sites for oxygen reduction as well.

The presence of moisture in air degrades LSM cathode performance by favoring segregation of $SrO/Sr(OH)_2$ at the surface and $La_2Zr_2O_7$ formation as well as MnO_x and La_2O_3 precipitation at the LSM-YSZ interface [21–23]. The degradation rate increases with cathodic bias and moisture content. The degradation rate is higher at 1023 K compared to ≥1123 K operating temperature [23]. The underlying mechanisms for the role of moisture on LSM degradation have been documented in previous studies [11,21].

CO_2 in air competes with O_2 for the active sites for ORR [24,25]. CO_2 tends to react with SrO at the LSM surface to form $SrCO_3$ [26]. Recently, it has been shown that small amount of CO_2 (<0.05%) in O_2 slightly decreases LSM performance [24]. Observable change in microstructure and electrochemical performance in nominal air containing ~400 ppm CO_2 would require long operating time. Therefore, higher concentrations of CO_2 (0.5–10%) in air are used in this study to identify LSM cathode degradation and subsequent microstructure changes within a reasonable testing period. We have systematically investigated the role of CO_2 in air on the LSM cathode by electrochemical testing as well as post-test analysis. Our study reveals that CO_2 initially degrades the LSM performance followed by a stable performance.

2. Experimental

2.1. Materials and experimental setup

LSM ($(La_{0.8}Sr_{0.2})_{0.98}MnO_3$) ink and YSZ ($(Y_2O_3)_{0.08}(ZrO_2)_{0.92}$) electrolyte (Fuel Cell Materials) were used for the fabrication of LSM/YSZ/LSM symmetrical cells. The LSM electrodes were screen-printed on both side of LSM (thickness: ~17 μm, diameter: 1.0 cm). Platinum mesh and wires (Alfa Aesar, wire diameter: 0.2 mm) and platinum paste (Engelhard) were used as electrode materials. The procedures for the cell fabrication and electrochemical testing have been described in our previous study [21].

As-fabricated LSM/YSZ/LSM cells were installed in a tubular alumina reaction chamber placed in the middle of a vertical tube furnace. The leads from a potentiostat (VMP2, Bio-Logic) were connected to the three platinum electrodes of the symmetrical cell. The schematic of the experimental setup for electrochemical testing is shown in Fig. 1. Dry air (CO_2 < 1 ppm) and 0.5–10% CO_2 containing dry air (certified Airgas) was introduced by a mass flow controller. For long-term stability tests, cells were tested in dry air and 0.5–10% CO_2–air, at 1023–1123 K temperature range in 0 V and 0.5 V cathodic biases up to 100 h.

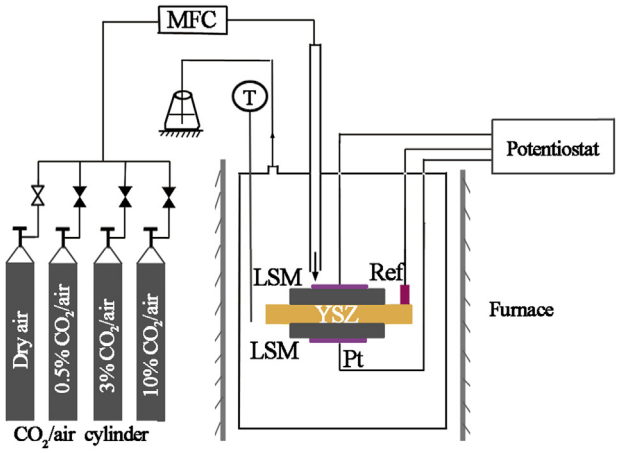

Fig. 1. Schematic for the experimental setup for the electrochemical test.

2.2. Characterization

A multi-channel potentiostat (VMP2, Bio-Logic) was used to record the real-time electrochemical impedance spectra (EIS) in the frequency range from 0.5 Hz to 200 kHz with 15 mV sinusoidal amplitude at an interval of 2 h.

An FEI Quanta 250 FEG scanning electron microscope attached with an energy dispersive X-ray spectroscope (EDS) was used for the morphological and elemental analyses. Fourier transform infrared (FTIR) spectra of standard $SrCO_3$ power (99.995%, Aldrich) and LSM films were recorded on a Nicole iS50 FT-IR spectrometer equipped with attenuated total reflectance (ATR) attachment, germanium crystal, and dedicated DLaTGS detector. Depth compositional profile analyses were performed on a PHI 595 multi-probe system using Auger electron spectroscopy (AES). A thin gold film (~5 nm) was coated on LSM surface to make it conductive. Ion beam sputtering was used to remove materials from the sample surface.

Thermo-gravimetric analyses (TGA) of SrO (99.5%), La_2O_3 (99.9%) and MnO_2 (99.9%)(Alfa Aesar) were performed using an NETZSCH Jupiter instrument (STA 449 F3) to identify the plausible mechanisms of LSM degradation as well as to complement the post-test analytical study. These oxides were pre-heated at 1173 K in dry air to remove adsorbed moisture, if any. After cooling down to room temperature, 10% CO_2–air was introduced to the chamber and the samples were reheated at 3 K min^{-1} up to 1173 K. Finally, the samples were cooled down to room temperature in 10% CO_2–air. The post-test samples were analyzed using a Bruker AXS D-8 Diffractometer (XRD).

3. Results

3.1. Electrochemical performance

Fig. 2 shows the effect of CO_2 concentration on the electrochemical performance of the LSM/YSZ/LSM symmetric cell at 1123 K under a cathodic bias of 0.5 V. With applying a bias of 0.5 V, the current densities of these symmetrical cells are closed to those of the large-scale SOFC stacks with LSM cathodes (0.8–1.8 A cm^{-2}) [2]. In 3% and 10% CO_2–air, the current density initially increases for

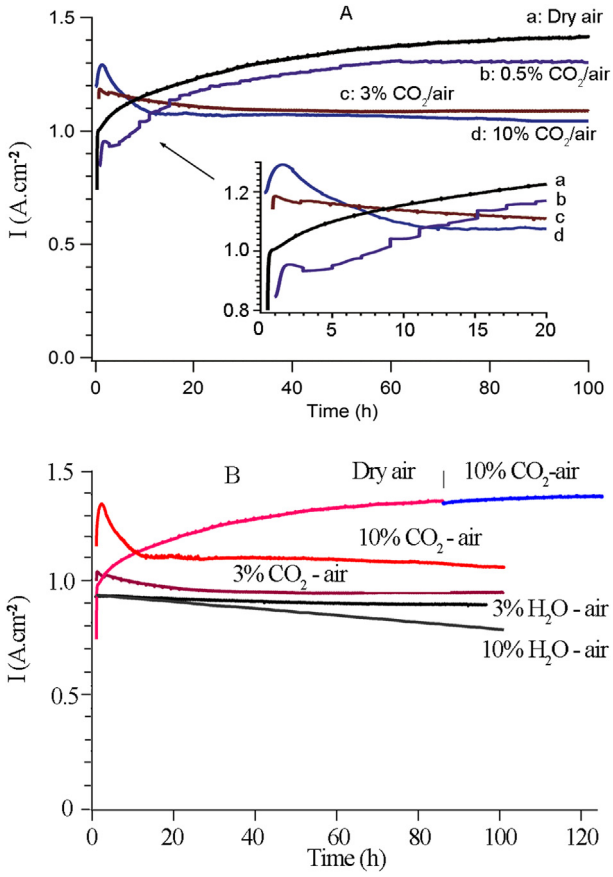

Fig. 2. *I–t* plots of the LSM/YSZ/LSM cells at 1123 K and 0.5 V bias. A: in air containing 0–10% CO_2 at 1123 K, B: activated in dry air and subsequently tested in 10% CO_2 - air, comparing to 10% CO_2–air, 3% CO_2–air, 3% H_2O–air, and 10% H_2O–air. *I–t* plots of the LSM/YSZ/LSM cells in H_2O–air are included here only to compare with the performance in CO_2–air. (The LSM degradation data in 3% H_2O–air and 10% H_2O–air are adapted from our previous study (Ref. [21])).

~2 h followed by decreasing up to ~20 h (inset in Fig. 2A) and then maintains almost a constant value for the remaining testing period. Higher the concentration of CO_2 in air, the initial change in current density is more prominent. The initial increase in current density is due to the activation process similar to the observation for the samples tested in air. It is observed that the cathode performance does not decrease after the activation process for the cells tested in air and/or low concentration (≤0.5%) of CO_2 in air. The cathode performance in 0.5% CO_2–air is comparable to that in dry air. It has also been noticed that the decrease in current density is negligible in 10% CO_2–air if the cell is already activated in air as shown in Fig. 2B. The cell has been activated in dry air for 85 h prior to introduction of 10% CO_2–air. The cathode performance in CO_2–air has been compared with that in H_2O–air in Fig. 2B. After the initial change within 20 h, the current density decreases by ~3.9×10^{-2} A cm^{-2} in 10% CO_2–air, ~3.7×10^{-3} A cm^{-2} in 3% CO_2–air, ~6.1×10^{-2} A cm^{-2} in 3% H_2O–air and ~0.17 A cm^{-2} in 10% H_2O–air. The performance degradation of the LSM cathode in H_2O–air is much faster than in the air containing the same concentration of CO_2.

The effect of the operating temperature on the cathode performance has been examined in 10% CO_2–air (Fig. 3) under 0.5 V cathodic bias. An increase in current density with increase in operating temperature is attributed to increased electrical conductivities of YSZ and LSM. After the initial changes observed within the first 20 h, the current density was observed to (i) remain

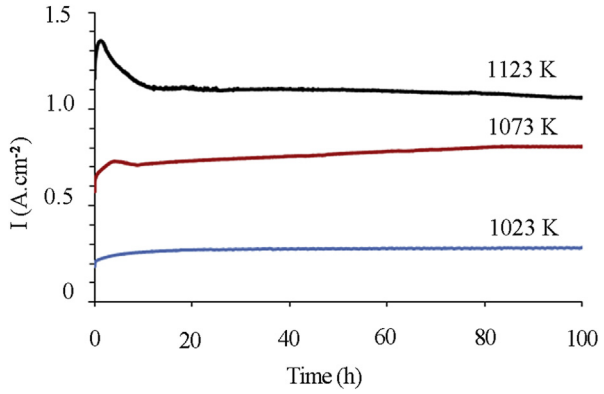

Fig. 3. *I–t* plots of the LSM/YSZ/LSM cells at 0.5 V in 10% CO_2– air in different operating temperatures.

steady at 1023 K, (ii) show a slight increase (4.4×10^{-2}) A cm^{-2} at 1073 K and (iii) a reduction (-3.9×10^{-2} A cm^{-2}) at 1123 K.

The non-ohmic and ohmic resistances determined from the electrochemical impedance spectra for the cells tested in dry air and CO_2–air is plotted as a function of time in Fig. 4. When LSM cathodes were polarized with a bias of 0.5 V at different CO_2 concentration, the non-ohmic resistances of the cathodes in CO_2 (3% and 0.5%) – air initially decreases faster than that in 10% CO_2–air. Three repeated experiments in 10% CO_2–air confirmed the same trend. After a certain testing period (40–80 h), all these cells maintain a constant non-ohmic resistance. The time to reach a constant non-ohmic resistance increases with increase in CO_2 concentration in air. Compared to the change in non-ohmic

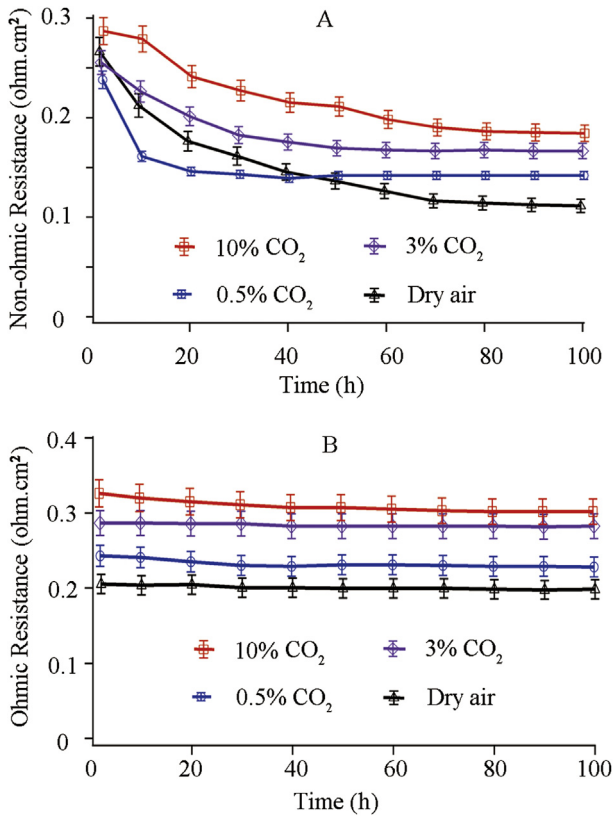

Fig. 4. *R–t* plots of LSM cathode. A: non-ohmic and B: ohmic resistances in air with different CO_2 concentration at 1123 K and 0.5 V bias.

resistance, the ohmic resistance of the same cell initially decreases slightly (Fig. 4B) and remains unchanged for the remaining testing period. Overall, both the non-ohmic and ohmic resistances increase with the increasing order of 10% CO_2–air > 3% CO_2–air > 0.5% CO_2–air > dry air.

Operating temperature also influences the ohmic and non-ohmic resistances of a cell tested in 10% CO_2–air as shown in Fig. 5. After an initial decrease, a continuous increase in the non-ohmic resistance with time at 1023 K and 1073 K was observed. A continuous decrease in the non-ohmic resistance has been observed during the first 70 h followed by a constant value for the cells tested at 1123 K. The ohmic resistances of the cells remain stable in all the studied temperatures but initially increased at 1073 K.

3.2. Post-test characterization

3.2.1. SEM

The SEM images of the LSM surfaces of the cells as-fabricated and exposed under 10% CO_2–air at 1023–1123 K for 100 h without applied bias are shown in Fig. 6. Segregated particles, identified as SrO in our earlier work [27], are observed on the LSM surface of the as-fabricated cell. After exposed in 10% CO_2–air for 100 h at 1023 K, larger particles were observed (Fig. 6B) on the LSM surface. The density of the particles at the LSM surface decreases with increasing temperatures (1073 and 1123 K). At 1023 K, the density of the segregated particles is comparable for the biased and unbiased samples (Fig. 6E).

Fig. 7 shows the SEM images of the LSM surfaces for the post-test samples tested in 0.5–10% CO_2–air at 1123 K with 0.5 V applied bias. The density of particles at the LSM surface increases with increase in CO_2 content in air. It is noticed by comparing Figs. 6D and 7F that the density of the particles at the LSM surface decreases but their size increases with an applied bias.

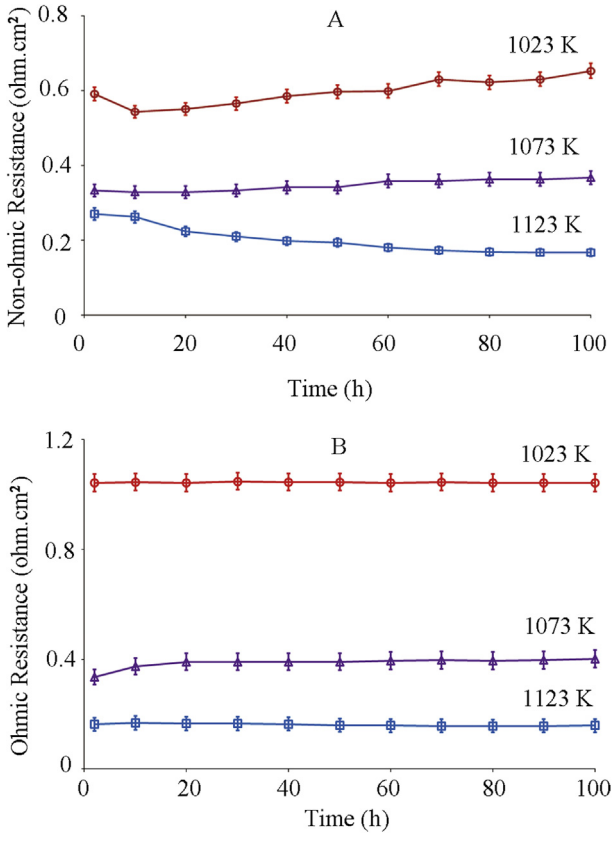

Fig. 5. *R–t* plots of the LSM cathode: non-ohmic and B: ohmic resistances at different operating temperatures at 10% CO_2–air and 0.5 V bias.

3.2.2. Auger electron spectroscopy

The elemental composition of the LSM surface and the subsurface of the tested cells was analyzed by AES technique to elucidate the compositional variation from the surface to the bulk. Fig. 8 shows the compositional depth profiles for the samples tested at 1023 K in 10% CO_2–air with applied biases of 0 V and 0.5 V, respectively. The samples exposed to 10% CO_2–air at 1023 K have been considered as the representative sample since the density of particles at the LSM surface is the highest. The compositional depth profile of the as-fabricated cell is also shown in Fig. 8A as a baseline. For the as-fabricated sample, the atomic percentage of strontium and carbon is higher at the surface indicating the presence of strontium carbonate at the LSM surface. Relatively lower amount of strontium is found at the surface for the samples tested with 0.5 V bias. This result is consistent with the lower density of surface particles compare to those for the samples tested with 0 V bias (Figs. 6D and 7F). More carbon has been observed for the biased samples indicating chemical adsorption on the oxygen vacancies. The increase of carbon is attributed to CO_2 adsorption and dissociation on oxygen vacancies (see discussion) [27,28]. Enrichment of strontium and carbon at the surface indicates the presence of strontium carbonate at the surface. The compositional depth profile shows that the formed carbonate extends to few nm in depth in the increasing order of 10% CO_2–air with 0.5 V bias > 10% CO_2–air with 0 V bias > as-fabricated.

3.2.3. ATR-FTIR spectra

Fig. 9 shows the ATR-FTIR spectra of standard $SrCO_3$ and the post-reaction LSM cathodes at 1123 K in 10% CO_2–air with a cathodic bias of 0.5 V. For the standard $SrCO_3$ sample, two bands at 1430 and 855 cm^{-1} are assigned to the C=O symmetric stretching and in-plane bending of CO_3^{2-} respectively [29].The transmission bands between 1350 and 1580 cm^{-1} are the diagnostics of carbonate minerals [29]. For the LSM cathode sample tested at 0.5 V and 1123 K in 10% CO_2–air, the band at 1430 cm^{-1} is associated with the C=O symmetric stretching of $SrCO_3$ and the band at 1370 cm^{-1} is attribute to unidentate carbonate formed in 10% CO_2–air at a high temperature of 1123 K [30]. The sharp peaks of $SrCO_3$ at 855 cm^{-1} is in-plane bending of CO_3^{2-} [29] and this peak shifts to 820 cm^{-1} for the $SrCO_3$ on LSM surface. It is also noted that the bands at 1370 cm^{-1} and 820 cm^{-1} could be assigned to lanthanum dioxycarbonate [31]. The presence of lanthanum dioxycarbonate is unlikely since an Auger electron spectrum (Fig. 8C) does not show lanthanum enrichment at the LSM surface.

3.2.4. Thermogravimetric analysis

Thermogravimetric analyses of the LSM and its constituent oxides were carried out to develop the mechanisms for the interaction of LSM with air and related effect on the electrochemical performance. SrO, La_2O_3, MnO_2, and LSM powders were heated in dry air and their weight loss is shown in Fig. 10A. As received SrO and La_2O_3 samples form metal hydroxides ($Sr(OH)_2$ and $La(OH)_3$) in the presence of moisture in the atmospheric air. On heating at 1173 K in dry air, these hydroxides convert into SrO and La_2O_3 [32] resulting in weight loss as shown in Fig. 10A. MnO_2 is converted to Mn_3O_4 at 823 K in dry air accompanied with a weight loss due to loss of lattice oxygen [33]. The weight loss of the LSM sample is due to loss of adsorbed water. After cooled down to room temperature, the oxides were exposed to 10% CO_2–air.

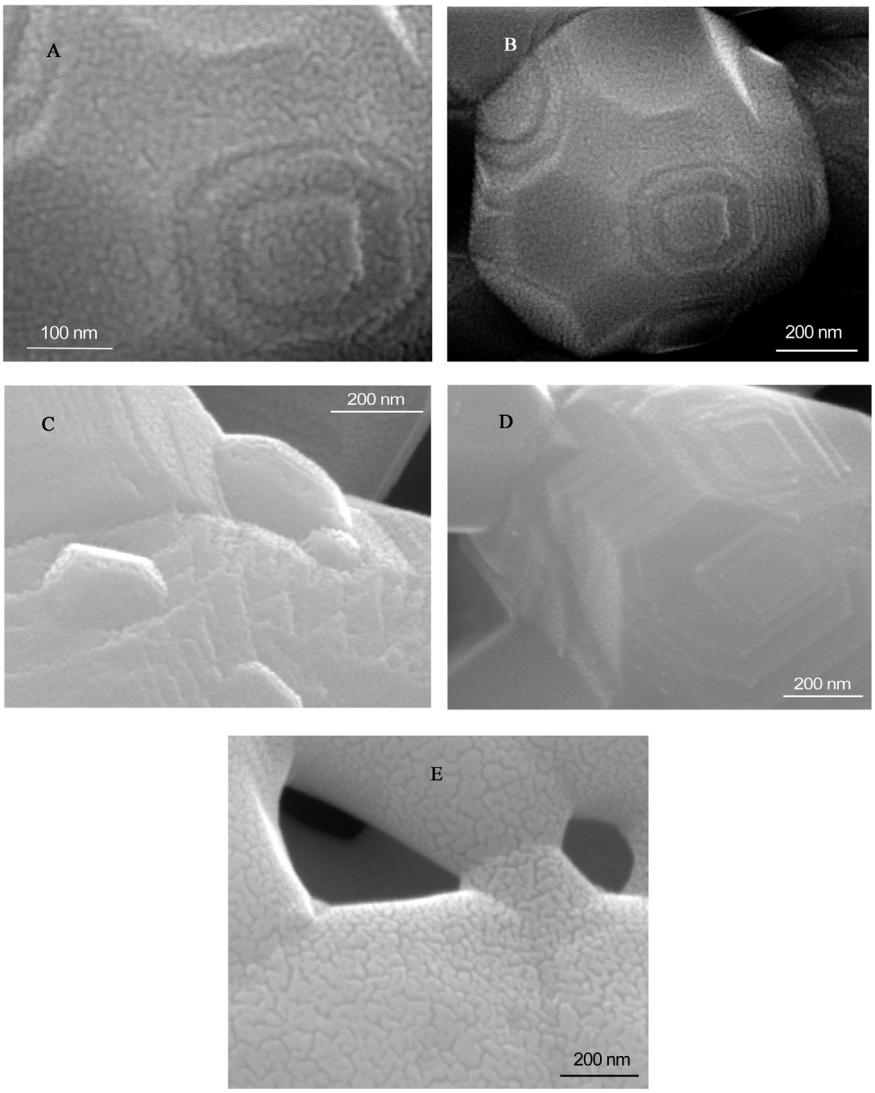

Fig. 6. SEM images of the post-test LSM cathodes in 10% CO_2–air at different temperatures. A: as-fabricated LSM in atmospheric air at 1473 K for 2 h; B, C, and D: exposed at 1023 K, 1073 K, and 1123 K respectively, 100 h, no bias, E: LSM cathode at 1023 K with a bias of 0.5 V for 100 h.

After these samples were exposed to 10% CO_2–air at high temperatures, SrO started to continuously gain weight from ~873 K to 1173 K; La_2O_3 started to gain weight from 823 K, maintained a constant weight between 923 and 1023 K, and then lost weight up to 1073 K [Fig. 10B]. The weight of LSM and Mn_2O_3 remained constant when heated from 298 to 1173 K in 10% CO_2–air [Fig. 10B].

The XRD patterns (Fig. 11) of these post-test samples show that SrO and La_2O_3 was converted to $SrCO_3$ and $La_2O_2CO_3$ in 10% CO_2–air, respectively. La_2O_3 was also heated at 1173 K for 1 h in dry air before introducing 10% CO_2–air. Comparing the XRD patterns of the pretest and post-test La_2O_3, some characteristic peaks of La_2O_3 disappeared with the remaining peaks matching the pattern of $La_2O_2CO_3$. $La_2O_2CO_3$ observed in the post-test sample of TGA formed during cooling in 10% CO_2–air. $La_2O_2CO_3$ decomposes at 1073 K in 10% CO_2–air (this study) while it decomposes at 1233 K and forms during cooling at 1093 K in pure CO_2 gas as reported by Bakiz et al. [34].

4. Discussion

The LSM cathode performance decreases with increase in CO_2 concentration in air during the initial testing period (~20 h) and then remains stable. In presence of CO_2 in air, the LSM cathode performance is much lower at 1023 K than those at 1073 K and 1123 K. Another notable observation is that the change in cathode performance mostly takes place in the initial testing period. These observations are explained below.

SrO segregation is often observed in LSM surface due to surface energetics [27,35]. CO_2 reacts with SrO and forms $SrCO_3$. The Gibbs free energies for the formation of the strontium carbonate (ΔG_{SrCO_3}) and lanthanum dioxycarbonate carbonates ($\Delta G_{La_2O_2CO_3}$) have been calculated according to the following reactions and shown in Table 1 at different CO_2 concentrations and temperatures [35].

$$SrO(s) + CO_2(g) \leftrightarrow SrCO_3(s) \quad (1)$$

and

$$La_2O_3(s) + CO_2(g) \leftrightarrow La_2O_2CO_3 \quad (2)$$

The formation of manganese carbonate is not thermodynamically favorable. As seen from Table 1, both the strontium carbonate and lanthanum dioxycarbonate is stable even at room temperature. It is also noticed that the carbonates do not remain stable above

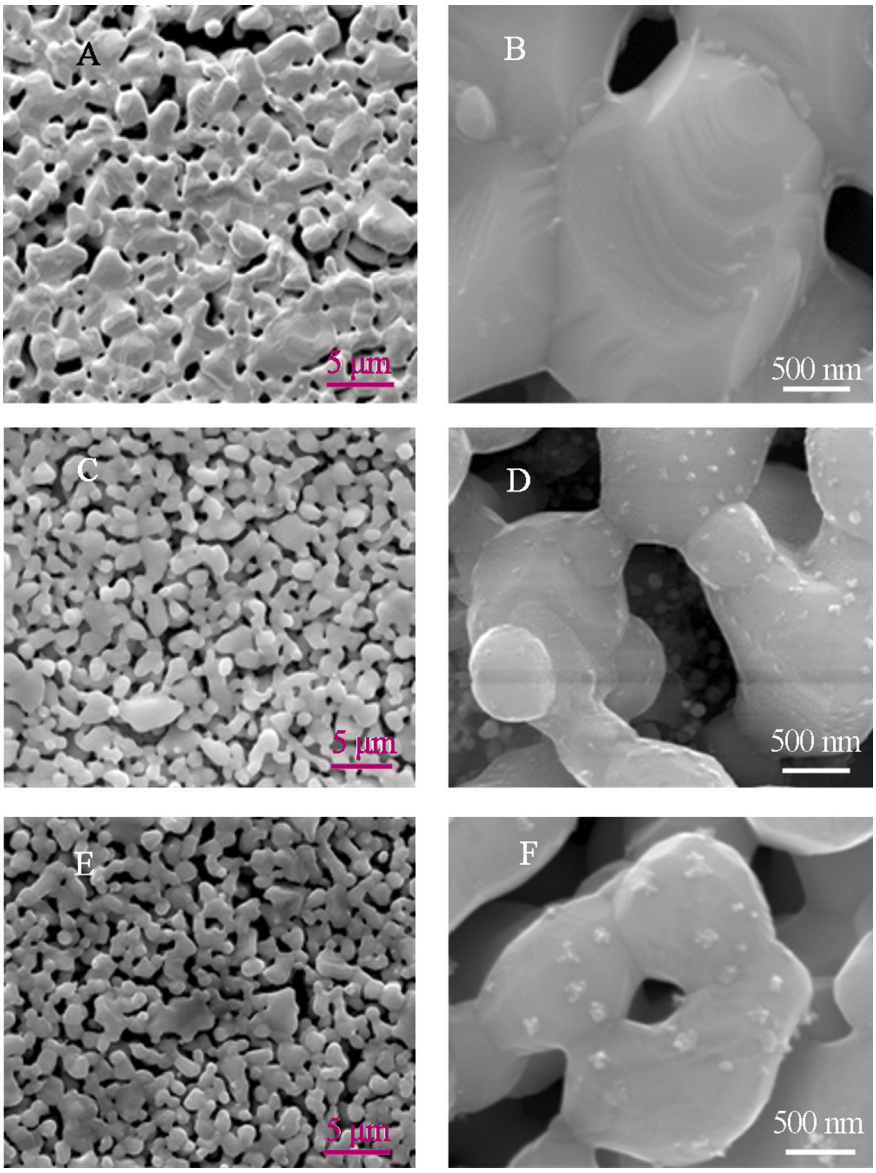

Fig. 7. SEM images of the post-test LSM cathodes at 0.5 V bias and 1123 K in air containing 0.5–10% CO_2. A/and B: 0.5% CO_2–air, C and D: 3% CO_2–air, E and F: 10% CO_2–air.

1000 K in atmospheric air (~400 ppm CO_2). TGA analysis shows that lanthanum carbonate dissociates at ~1073 K while strontium carbonate remains stable in the studied temperatures, consistent with the formation energies at 10% CO_2–air. The decomposition temperature of $SrCO_3$ in 1 atm CO_2 is 1426 K as calculated from Barin et al. [36], while Murthy et al. [37] observed 1533 K in their TGA study.

Along with $SrCO_3$, lanthanum carbonate is likely to be present at the LSM surface for 1023 K testing temperature resulting in lower performance than at the higher temperatures. As a result, the density of particles at the LSM surface decreases with temperature increase (Fig. 6). In addition to the higher density of carbonates, the lower electrical conductivities of LSM and YSZ at <1073 K contribute for the lower performance at 1023 K.

The underlying mechanisms for the LSM cathode performance during the initial testing period are proposed from the experimental observations. The proposed mechanisms are shown schematically in Fig. 12. SrO in the LSM surface reacts with CO_2 to form $SrCO_3$. Formation of $SrCO_3$ is thermodynamically driven as supported by its presence in the as-fabricated LSM cathodes and increased $SrCO_3$ with CO_2 concentration in air.

Observation I: The electrochemical performance of LSM cathode initially increases in CO_2–air.

It is known that the LSM surface is SrO enriched [38]. The change in cathode performance during initial testing in CO_2–air can be explained similarly as LSM activation mechanism in dry air. With cathodic bias (0.5 V), SrO incorporates into the LSM lattice [20,39] and oxygen vacancies form at the LSM according to

$$V'''_{La,LSM} + SrO + 3Mn^{\bullet}_{Mn,SM} + e' \leftrightarrow Sr'_{La,LSM} + O^{x}_{o,YSZ} + 3Mn^{x}_{Mn,LSM} \quad (3)$$

$$O^{x}_{O,LSM} + 2Mn^{x}_{Mn,LSM} + V^{\bullet\bullet}_{O,YSZ} + 2e' \leftrightarrow V^{\bullet\bullet}_{O,LSM} + 2Mn'_{Mn,LSM} + O^{x}_{O,YSZ} \quad (4)$$

Where $V'''_{La,\ LSM}$, $Mn^{\bullet}_{Mn,\ LSM}$, and $Mn^{x}_{Mn,\ LSM}$, and $Sr'_{La,\ LSM}$ represent cation vacancies, Mn^{4+} and Mn^{3+} ions, and strontium on lanthanum sites in LSM lattice, respectively. $V^{\bullet\bullet}_{O,YSZ}$, $V^{\bullet\bullet}_{O,LSM}$, and

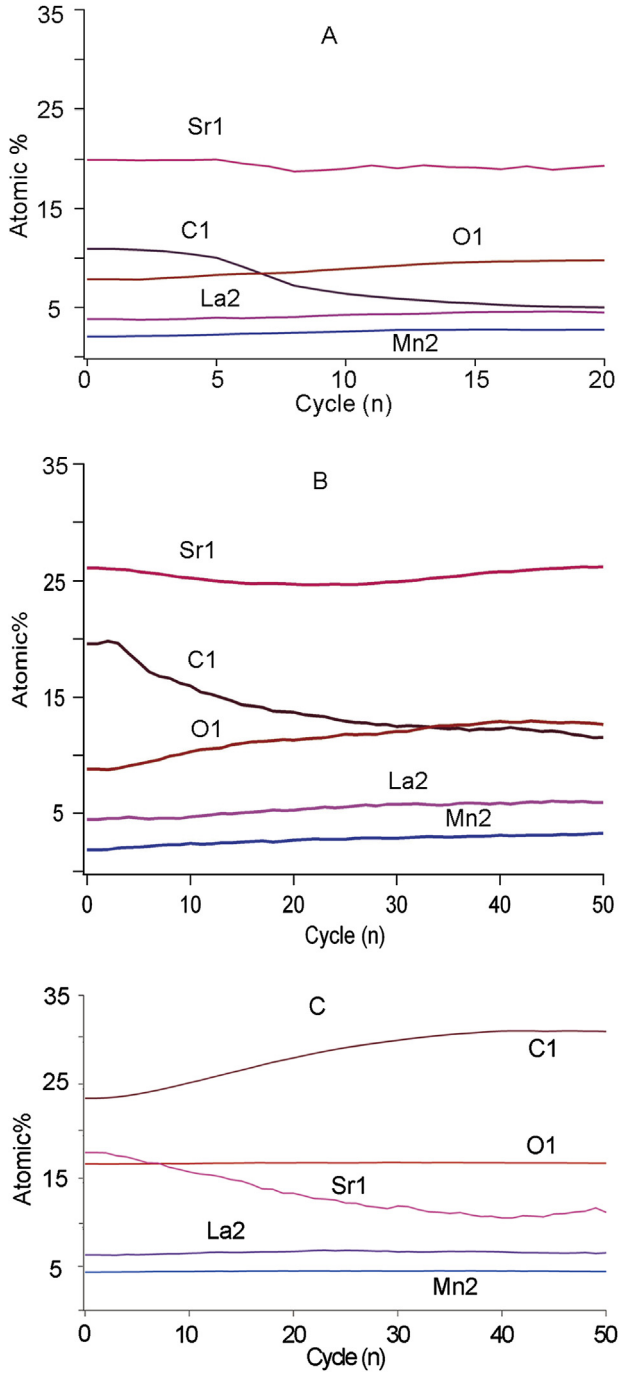

Fig. 8. AES depth compositional profiles of pretest and post-test LSM cathodes. A: pretest LSM sintered in air for 2 h at 1473 K, B: LSM (no bias), C: LSM (bias: 0.5 V) exposed in 10% CO_2–air at 1023 K for 100 h.

$O^{x}_{O,YSZ}$ represent oxygen vacancies in YSZ and LSM lattice and oxygen in YSZ lattice oxygen sites, respectively.

CO_2 competes with O_2 in air in a similar manner for dissociative adsorption at the oxygen vacancy sites as reported for LSCF and $La_{0.2}Sr_{0.8}Ti_{0.9}Mn_{0.1}O_{3+\delta}$ samples [39,40]. Enhanced surface exchange and oxygen diffusivity has been identified in LSCF cathode in presence of CO_2 and H_2O in air [39]. The competing nature of CO_2 adsorption with O_2 has also been observed for LSM cathode [24]. Accordingly, the CO_2 may also enhance the dissociative adsorption similar to that of LSCF. As a result, the electrochemical performance

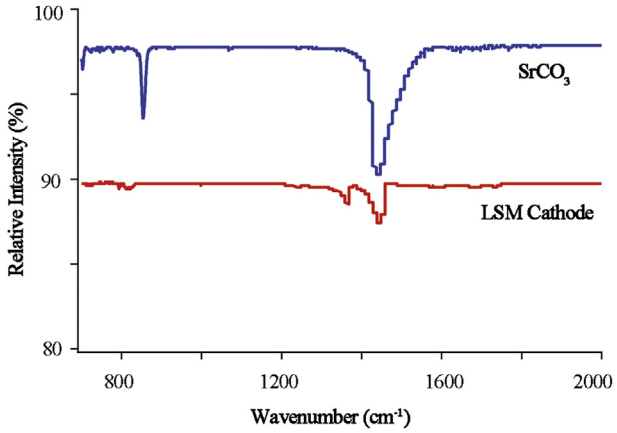

Fig. 9. ATR-FTIR spectra of standard $SrCO_3$ and post-reaction LSM cathodes (at 1123 K in 10% CO_2–air with 0.5 V cathodic bias).

initially increases. Higher concentration of carbon, but not strontium, in the AES depth compositional profile the biased sample than those for the unbiased samples (Fig. 8), supports the adsorption of CO_2 at oxygen vacancy sites.

Observation II: The electrochemical performance of LSM decreases after initial activation and remains unchanged for the remaining test period.

The cathode performance largely depends on the oxygen reduction rate which is significant at the topmost layer of the LSM

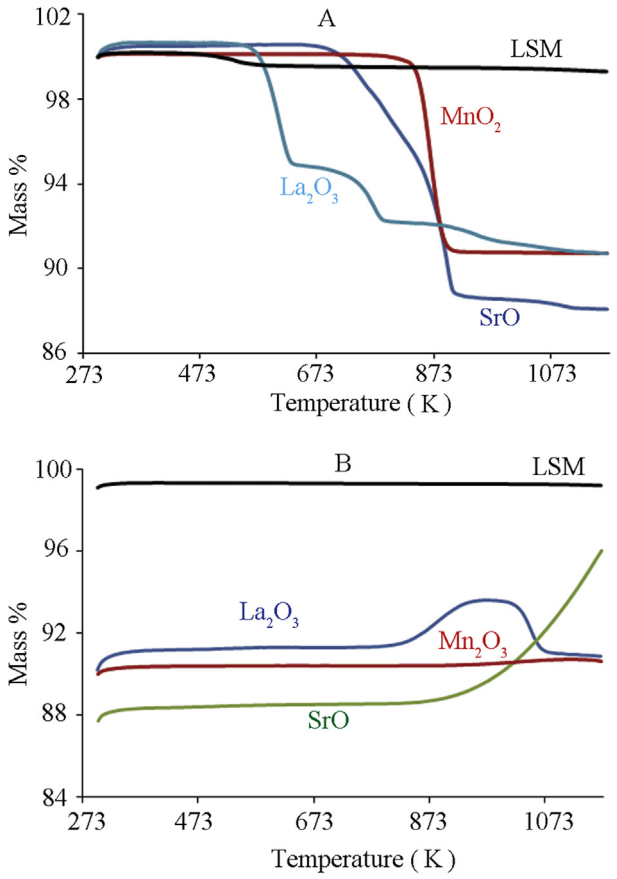

Fig. 10. TGA graph of LSM and its precursor oxides exposed in dry air (A) and then in 10% CO_2–air (B).

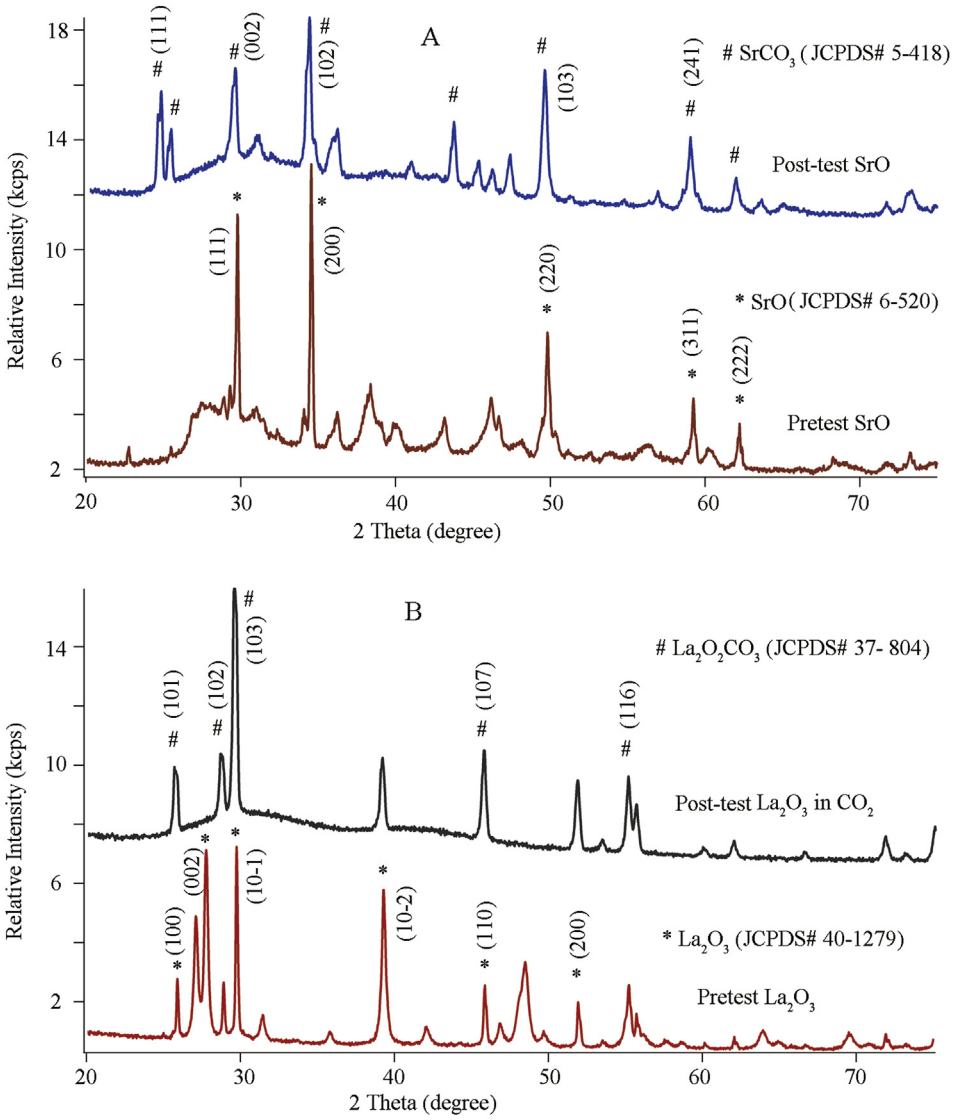

Fig. 11. XRD patterns of pre-test and post-test La_2O_3 and SrO in TGA.

surface. SrO at the surface reacts with CO_2 to form $SrCO_3$ simultaneously with the CO_2 adsorption at oxygen vacancies. $SrCO_3$ at the surface may block oxygen adsorption sites and subsequent desorption, decreasing the cathode performance.

Once the SrO at the surface is completely incorporated into the LSM lattice during activation stage, no more $SrCO_3$ may form at the surface to block sites for oxygen reduction reaction. As a result, the performance does not degrade further with time.

Observation III: The electrochemical performance of LSM does not decrease in CO_2–air for the samples pre-activated in air (Fig. 2B).

Table 1
Gibbs free energy of strontium carbonate ($SrCO_3$) and lanthanum dioxycarbonate ($La_2O_2CO_3$) formation.

Temperature (K)	298	400	600	800	900	1000	1100	1200
ΔG_{SrCO_3} (kJ mol^{-1})[a]	−189.2	−171.7	−137.9	−104.6	−88.2	−71.9	−55.9	−40.1
ΔG_{SrCO_3} (kJ mol^{-1})[b]	−183.5	−164.0	−126.4	−89.3	−71.0	−52.8	−34.9	−17.1
ΔG_{SrCO_3} (kJ mol^{-1})[c]	−163.0	−136.5	−85.1	−30.4	−8.9	16.2	41.0	65.6
$\Delta G_{La_2O_2CO_3}$ (kJ mol^{-1})[a]	−147.3	−130.0	−96.4	−63.6	−47.4	−31.6	−15.9	−0.5
$\Delta G_{La_2O_2CO_3}$ (kJ mol^{-1})[b]	−141.6	−122.4	−84.9	−48.3	−30.2	−12.5	5.1	22.5
$\Delta G_{La_2O_2CO_3}$ (kJ mol^{-1})[c]	−121.1	−94.8	−43.6	6.8	31.9	56.5	81.0	105.2

For 1 atm pure CO_2, ΔG_{SrCO_3} was calculated by HSC Chemistry 6.0. $\Delta G_{La_2O_2CO_3}$ data are adapted from Ref. [35]. For the data of b and c, they are calculated based on equation: $\Delta G = -RT\ln P_1/P_{1\ atm}$. Where R is the ideal gas constant = 8.314 J mol^{-1}. K^{-1}, T is the absolute temperature (K), P_1 is the partial pressure of CO_2 in the gas, and ΔG is the Gibbs free energy change.

[a] In 1 atm pure CO_2.
[b] In 10% CO_2–air.
[c] In 400 ppm CO_2–air.

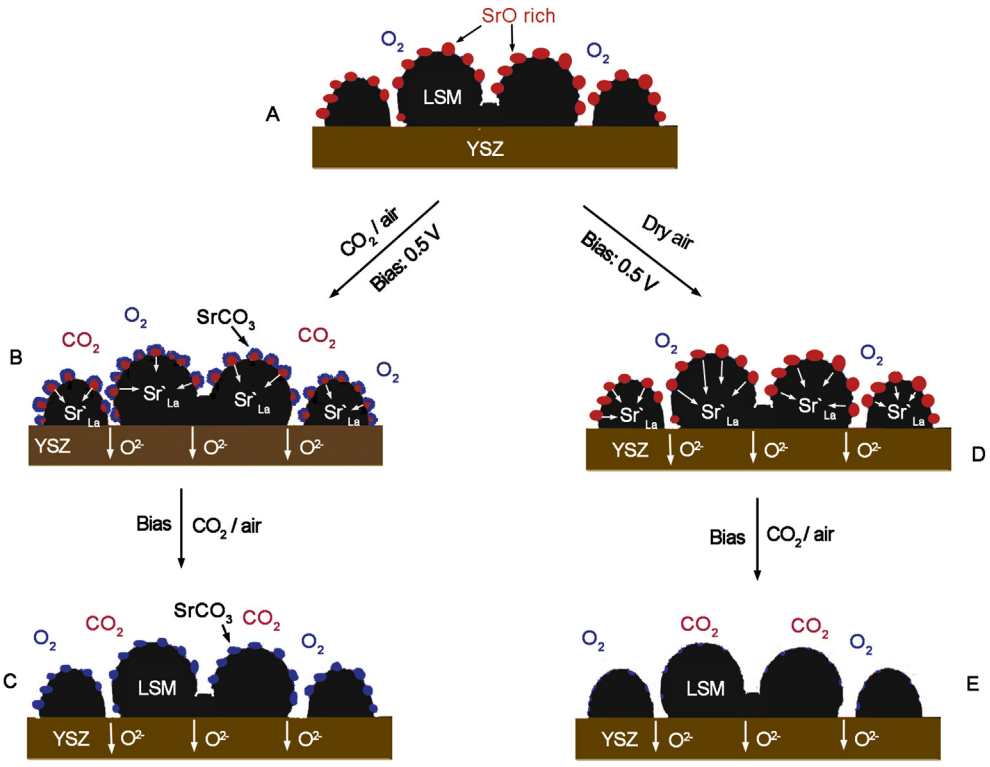

Fig. 12. Schematic of the mechanisms of CO_2 interaction with LSM and related electrochemical performance. A: as-fabricated LSM cathode; B: partial incorporation of SrO into the LSM lattice and formation $SrCO_3$ at the LSM surface; limited activation and performance degradation, C: increased $SrCO_3$ on the surface and subsequent performance degradation; D: SrO incorporation into the LSM lattice; LSM activation in dry air. E: No more $SrCO_3$ formation at the LSM surface due to absence of SrO; stable electrochemical performance.

After the activation of LSM in air for 85 h, the $SrCO_3$ content will not increase due to absence of SrO at the LSM surface. As a result, the electrochemical performance does not decrease.

5. Conclusions

Role of carbon dioxide on the lanthanum strontium manganite (LSM) cathode performance has been investigated in the temperature range of 1023–1123 K with 0 V and 0.5 V cathodic bias. The degradation in the electrochemical performance of the LSM cathode is negligible after initial operation period of ~20 h. The formation of $SrCO_3$ at the LSM surface is responsible for the initial stage degradation in CO_2 containing air. This study shows that the presence of CO_2 in air does not affect the electrochemical performance of the LSM cathode pre-activated in air for 85 h. A mechanism has been developed to support the experimental observations.

Acknowledgments

This study was performed under a grant from the Office of Fossil Energy, US Department of Energy (grant number: DE-FE-0009682). Technical discussion with Dr. Jeff Stevenson at the Pacific Northwest National Laboratory is acknowledged. Mr. David Kriz, PhD candidate in the Department of Chemistry, University of Connecticut is acknowledged for AES sample preparation.

References

[1] H.C. Maru, S.C. Singhal, C. Stone, D. Wheeler, 1–10 kW Stationary Combined Heat and Power Systems Status and Technical Potential: Independent Review, Tech. Rep. NREL/BK-6A10-48265, NREL, Golden, CO, 2010, http://dx.doi.org/10.2172/993647.
[2] L. Blum, L.G.J. de Haart, J. Malzbender, N.H. Menzler, J. Remmel, R. Steinberger-Wilckens, J. Power Sources 241 (2013) 477–485.
[3] R.J. Bratton, L.J.H. Kuo, R.J. Ruka, P. Singh, US Patent 5,686,198, 1997.
[4] X.Y. Lou, Z. Liu, S.Z. Wang, Y.H. Xiu, C.P. Wong, M.L. Liu, J. Power Sources 195 (2010) 419–424.
[5] J. Malzbender, P. Batfalsky, R. Vassen, V. Shemet, F. Tietz, J. Power Sources 201 (2012) 196–203.
[6] M.K. Mahapatra, P. Singh, in: T.M. Letcher (Ed.), Future Energy, Elsevier, Waltham, MA, 2014, pp. 511–544.
[7] M.K. Mahapatra, S. Bhowmick, N. Li, P. Singh, J. Eur. Ceram. Soc. 32 (2012) 2341–2349.
[8] H. Yokokawa, H.Y. Tu, B. Iwanschitz, A. Mai, J. Power Sources 182 (2008) 400–412.
[9] M. Backhaus-Ricoult, Solid State Ionics 179 (2008) 891–895.
[10] N. Li, M.K. Mahapatra, P. Singh, J. Power Sources 221 (2013) 57–63.
[11] J. Nielsen, M. Mogensen, Solid State Ionics 189 (2011) 74–81.
[12] H. Yokokawa, T. Horita, K. Yamaji, H. Kishimoto, T. Yamamoto, M. Yoshikawa, Y. Mugikura, K. Tomida, Fuel Cells 13 (2013) 526–535.
[13] P. Tans, NOAA/ESRL, www.esrl.noaa.gov/gmd/ccgg/trends/, R. Keeling, Scripps Institution of Oceanography, scrippsco2.ucsd.edu/, March 5, 2014.
[14] U.S. EPA, National Trends in Sulfur Dioxide Levels, www.epa.gov/airtrends/sulfur.html, March 5, 2014.
[15] M.K. Mahapatra, K. Lu, Mater. Sci. Eng. R 67 (2010) 65–85.
[16] Y.H. Li, R. Gemmen, X.B. Liu, J. Power Sources 195 (2010) 3345–3358.
[17] E.J. Crumlin, E. Mutoro, S.J. Ahn, G.J. la O', D.N. Leonard, A. Borisevich, M.D. Biegalski, H.M. Christen, Y. Shao-Horn, J. Phys. Chem. Lett. 1 (2010) 3149–3155.
[18] N. Caillol, M. Pijolat, E. Siebert, Appl. Surf. Sci. 253 (2007) 4641–4648.
[19] W. Jung, H.L. Tuller, Energy Environ. Sci. 5 (2012) 5370–5378.
[20] A.K. Huber, M. Falk, M. Rohnke, B. Luerssen, M. Amati, L. Gregoratti, D. Hesse, J. Janek, J. Catal. 294 (2012) 79–88.
[21] B. Hu, M. Keane, M.K. Mahapatra, P. Singh, J. Power Sources 248 (2014) 196–204.
[22] T.A. Jin, K. Lu, J. Power Sources 197 (2012) 20–27.
[23] A. Hagen, K. Neufeld, Y.L. Liu, J. Electrochem. Soc. 157 (2010) 1343–1348.
[24] Z. Zhao, L. Liu, X.M. Zhang, W.M. Wu, B.F. Tu, D.R. Ou, M.J. Cheng, J. Power Sources 222 (2013) 542–553.
[25] R. Hammami, H. Batis, C. Minot, Surf. Sci. 603 (2009) 3057–3067.
[26] S. Ponce, M.A. Pena, J.L.G. Fierro, Appl. Catal. B Environ. 24 (2000) 193–205.
[27] R. Bertacco, J.P. Contour, A. Barthelemy, J. Olivier, Surf. Sci. 511 (2002) 366–372.
[28] K. Suvegh, K. Nomura, G. Juhasz, Z. Homonnay, A. Vertes, Radiat. Phys. Chem. 58 (2000) 733–736.
[29] J. Coates, in: R.A. Meyers (Ed.), Encyclopedia of Analytical Chemistry, Wiley, Chichester, 2000, pp. 10815–10837.
[30] C.H. Rochester, M.S. Scurrell, Infrared Studies of Species Adsorbed on Oxide Surface, RSC Publishing, 1973.

[31] Q. Mu, Y. Wang, J. Alloys Compd. 509 (2011) 396–401.
[32] M. Aghazadeh, A.N. Golikand, M. Ghaemi, T. Yousefi, J. Electrochem. Soc. 158 (2011) 136–141.
[33] X. Chen, Y.F. Shen, S.L. Suib, C.L. O'Young, Chem. Mater. 14 (2002) 940–948.
[34] B. Bakiz, F. Guinneton, M. Arab, A. Benlhachemi, S. Villain, P. Satre, J.R. Gavarri, Adv. Mater. Sci. Eng. (2010), http://dx.doi.org/10.1155/2010/360597.
[35] A. Olafsen Sjåstad, H. Fjellvåg, K.B. Helean, A. Navrotsky, Themochim. Acta 550 (2012) 76–82.
[36] I. Barin, Thermochemical Data of Pure Substances, third ed., Wiley, 2008.
[37] S.R. Murthy, B.L. Newalkar, S. Kornarneni, in: D. Bahadur, S. Vitta, O. Prakash (Eds.), Inorganic Materials: Recent Advances, Narosa Pub. House, New Delhi, 2004, pp. 153–155.
[38] S.P. Jiang, J. Solid State Electrochem. 11 (2007) 93–102.
[39] S.J. Benson, D. Waller, J.A. Kilner, J. Electrochem. Soc. 146 (1999) 1305–1309.
[40] W. Qi, Y. Gan, D. Yin, Z. Li, G. Wu, K. Xie, Y. Wu, J. Mater. Chem. A (2014) 6904–6915.